Ocean Modelling 121 (2018) 19–33

Contents lists available at ScienceDirect

Ocean Modelling

journal homepage: www.elsevier.com/locate/ocemod

Estimating the numerical diapycnal mixing in an eddy-permitting ocean model

Alex Megann

National Oceanography Centre, Empress Dock, European Way, Southampton SO14 3ZH, United Kingdom

ARTICLE INFO

Keywords:
Global ocean
Ocean model
Numerical mixing
Watermass transformation

ABSTRACT

Constant-depth (or "*z*-coordinate") ocean models such as MOM4 and NEMO have become the de facto workhorse in climate applications, having attained a mature stage in their development and are well understood. A generic shortcoming of this model type, however, is a tendency for the advection scheme to produce unphysical numerical diapycnal mixing, which in some cases may exceed the explicitly parameterised mixing based on observed physical processes, and this is likely to have effects on the long-timescale evolution of the simulated climate system. Despite this, few quantitative estimates have been made of the typical magnitude of the effective diapycnal diffusivity due to numerical mixing in these models. GO5.0 is a recent ocean model configuration developed jointly by the UK Met Office and the National Oceanography Centre. It forms the ocean component of the GC2 climate model, and is closely related to the ocean component of the UKESM1 Earth System Model, the UK's contribution to the CMIP6 model intercomparison. GO5.0 uses version 3.4 of the NEMO model, on the ORCA025 global tripolar grid. An approach to quantifying the numerical diapycnal mixing in this model, based on the isopycnal watermass analysis of Lee et al. (2002), is described, and the estimates thereby obtained of the effective diapycnal diffusivity in GO5.0 are compared with the values of the explicit diffusivity used by the model. It is shown that the effective mixing in this model configuration is up to an order of magnitude higher than the explicit mixing in much of the ocean interior, implying that mixing in the model below the mixed layer is largely dominated by numerical mixing. This is likely to have adverse consequences for the representation of heat uptake in climate models intended for decadal climate projections, and in particular is highly relevant to the interpretation of the CMIP6 class of climate models, many of which use constant-depth ocean models at ¼° resolution

1. Introduction

The importance of using a correct distribution of the diapycnal mixing, and hence of the watermass transformation rate, to the large-scale ocean circulation in climate models is evident: the upwelling regions of the global overturning streamfunction are associated with mixing processes (Munk and Wunsch, 1998), while the formation of a realistic thermocline relies on appropriate rates of mixing above and below the thermocline (Luyten et al., 1983). In addition, the uptake of CO_2 and heat, both in the quasi-equilibrium state of control simulations and in simulations of anthropogenic warming, will be sensitive to the ocean stratification, while embedded biogeochemical systems will also have rather different mean states if the vertical mixing, and hence the stratification, are inconsistent with those in the real ocean. Small-scale turbulent mixing in ocean models is represented by a variety of parameterisations, including bulk schemes (e.g. Kraus and Turner, 1967), the KPP scheme (Large et al., 1994) and the turbulent kinetic energy (TKE) scheme (Gaspar et al., 1990); in these schemes, parameters are normally optimised in a more-or-less heuristic way to approximately reproduce the observed water mass structure.

So-called depth-coordinate ocean models, which represent the ocean as a stack of levels with constant vertical thickness, constitute the majority of ocean models used today: leading examples are NEMO (Madec, 2016) and version 4 of the GFDL Modular Ocean Model (MOM4, Griffies et al., 2008). We note that of the thirty-nine climate models contributing to the Intergovernmental Panel on Climate Change (IPCC) Fifth Assessment Report (IPCC, 2013), thirty-two used ocean components formulated with depth coordinates, three used terrain-following (sigma) coordinates, and four used an isopycnic (density-coordinate) ocean model. Numerical diapycnal mixing is an intrinsic property of the advection scheme in this class of models, and occurs whenever an advective flux crosses density surfaces, which in general do not follow the horizontal coordinate surfaces (Griffies et al., 2000). It may be reduced by the use of higher-order advection schemes (Hofmann and Morales Maqueda, 2006), and is absent, by construction, in the ocean interior in pure isopycnic models like MICOM (Bleck and

E-mail address: apm@noc.ac.uk.

https://doi.org/10.1016/j.ocemod.2017.11.001
Received 6 July 2017; Received in revised form 24 October 2017; Accepted 6 November 2017
Available online 14 November 2017

Smith, 1990) and GOLD (Hallberg and Adcroft, 2009), where advection is along surfaces of constant potential density and diapycnal mixing occurs only as prescribed by the model mixing scheme.

There are indications that in some regimes the numerical mixing may be of comparable magnitude as (and even exceed) the mixing generated by the explicit mixing scheme of the model (Griffies et al., 2000; Lee et al., 2002). This leads over time to the unrealistic modification of critical watermasses, which is likely to have undesirable effects on timescales of a decade or longer, and this may be critical in climate simulations. Megann et al. (2010) carried out a comparison between the coupled climate models HadCM3 and CHIME, which differ only in that in the latter the depth-coordinate ocean component of HadCM3 is replaced with the hybrid isopycnic-coordinate HYCOM (Bleck, 2002). The model with an isopycnic ocean showed markedly superior representation of watermasses such as Antarctic Intermediate Water (AAIW) and Subantarctic Mode Water (SAMW), as well as of the subtropical thermoclines and the sill overflow waters in the North Atlantic, all consistent with substantially lower numerical mixing. A similar conclusion was reached in a similar experiment with two coupled models at GFDL, differing only in the replacement in one of the MOM4 ocean model by the GOLD isopycnic-coordinate model (Dunne et al., 2012).

Several approaches to diagnosing the numerical mixing in ocean models have been developed in recent years. Firstly there are what we might call “direct” methods, which evaluate the mixing generated by the advection scheme at each grid cell: these include the use of passive tracers (Getzlaff et al., 2012); and analysis of tracer variance decay (Burchard and Rennau, 2008). These may be distinguished from more indirect methods, which diagnose the effects of mixing over global or basin-scale spatial domains, and over time scales long compared with the model time step: these include the evaluation of changes in global available potential energy (Ilıcak et al., 2012) and the estimation of diapycnal mixing by evaluating fluxes across density surfaces (Lee et al., 2002).

The representation of the overturning circulation in density space (Walin, 1982) is potentially highly revealing of the mechanisms of watermass transformation. Marsh et al. (2000) used an isopycnic (density-coordinate) model to show that changes in density arising from surface buoyancy fluxes (which in a Lagrangian sense generally act to increase the density of water as it is advected poleward) are balanced by changes in density resulting from diffusive mixing in the ocean interior. Marsh (2000), and subsequently Grist et al. (2009), showed that surface fluxes, when cast into density classes, provide an informative proxy for the overturning circulation, where the latter is not trivial to estimate directly from the relatively sparse direct observations of the ocean interior. Lee et al. (2002) used this framework to diagnose the interior diapycnal mixing in the OCCAM ¼° global ocean model, and then, by relating this to the mean vertical density gradient, to estimate the effective vertical diffusivity as a function of density and latitude. They concluded that in the Southern Ocean the effects of numerical mixing led to values of the effective diffusivity that were large compared with those applied by the parameterised vertical mixing scheme in the model.

In this paper we use the technique of Lee et al. (2002) to analyse the contributions to watermass transformation in the GO5.0 ocean model, the configuration of the NEMO code used in the GC2 coupled climate model (Williams et al., 2015), and closely related to the ocean configuration of the UK Earth System Model UKESM1 that will be used in the CMIP6 intercomparison. This model will be shown to have a rather lower drift than OCCAM, as used by the former authors. We shall use a modified version of the method used by Lee et al. to derive an estimate of the numerical diffusivity that is compared with the explicit mixing coefficients used in the model. Where these latter authors examined the numerical mixing in the southern hemisphere, with a primary focus on the Southern Ocean, we evaluate the diapycnal transformation rates and effective diffusivities globally, as well as separately in the Atlantic and Indo-Pacific Oceans.

In Section 2 we describe the GO5.0 model configuration. In Section 3 we summarise the methodology of Lee et al. (2002), and describe the numerical method used in the current paper. In Section 4 we present the results of this method applied to the model output, deriving the diapycnal velocities and effective diffusivities, and comparing these with the explicit diffusivities applied by the model's mixing scheme. In Section 5 we relate the diapycnal mixing to small-scale vertical motions, and finally Section 6 is a summary and discussion.

2. Model description

The model configuration we describe here is GO5.0 (Megann et al., 2014), a standard ocean configuration developed jointly between the UK Met Office and the National Environment Research Council (NERC). It is used widely in forecasting and climate modelling: the current version of the UK Met Office's FOAM operational ocean forecasting system (Blockley et al., 2014) and the UK coupled climate model GC2 (Williams et al., 2015) use GO5.0 as their ocean component. The GC3 climate model (Williams et al., 2017) and the new UK Earth System Model UKESM1, both aimed at the IPCC Sixth Assessment Report, will both use an ocean component closely related to GO5.0, in particular sharing its horizontal and vertical grids (albeit with a southward extension in the more recent configurations to allow ice shelves to be simulated) and most of its physics choices.

GO5.0 is an implementation of version 3.4 of NEMO (Nucleus for European Models of the Ocean, Madec, 2016) on the global ORCA025 0.25° tripolar horizontal grid (Barnier et al., 2006), and has 75 constant-depth levels in the vertical, with level spacing increasing from 1 m at the surface to around 200 m at 6000 m depth. The parameters and physics choices are discussed in detail in Megann et al. (2014). The sea ice is version 4.1 of the Los Alamos National Laboratory sea ice model CICE (Hunke and Lipscomb, 2010). The integration described here is of the ocean-only GO5.0 model forced by CORE2 atmospheric fields (Large and Yeager, 2009), and is made over the 30 years from 1976 to 2005. Monthly precipitation and daily downward shortwave and longwave radiation are used to force the model directly, while six-hourly 10-m wind, 2-m air humidity and 2-m air temperature are used to compute turbulent air–sea and air–sea–ice fluxes during model integration, using the bulk formulae proposed by Large and Yeager (2009). This configuration has much higher horizontal and vertical resolutions than the ocean of HadCM3, so should permit much better representation of watermasses, but still includes the fundamental process of advection across density surfaces characteristic of this model type, and indeed Griffies et al. (2000) suggest that models with eddy-permitting or eddy-resolving resolutions may have higher numerical mixing because of the vertical motions associated with the eddies.

GO5.0 uses the total variance dissipation (TVD) scheme (Zalesak, 1979) for horizontal advection of tracers. The vertical mixing of tracers and momentum in the GO5.0 configuration is parameterised using a modified version of the Gaspar et al. (1990) turbulent kinetic energy (TKE) scheme (described in Madec, 2016). Unresolved vertical mixing processes are represented by a background vertical eddy diffusivity (controlled by the parameter *rn_avt0* in NEMO) which has a constant value of 1.2×10^{-5} m^2 s^{-1} at latitudes poleward of ± 15°, decreasing linearly to a value of 1.2×10^{-6} m^2 s^{-1} at ± 5° latitude (Gregg et al., 2003). This parameter imposes an absolute minimum value for the diffusivity at each grid point, and the contributions of other processes such as double diffusion and breaking internal waves are represented by positive-definite increments to this. In regimes where the vertical density profile is unstable, convection is simulated by an enhanced vertical diffusivity for tracers and momentum of 10 m^2 s^{-1}. The time-averaged value of the applied explicit vertical diffusivity is saved at each grid point in the routine model output. GO5.0 uses the UNESCO equation of state for seawater (Chen and Millero, 1987) as implemented by Jackett and McDougall (1995).

We note that the 6-hourly surface forcing applied to the model means that our results are more directly comparable with those for the model run "6HW" in the study of Lee et al. (2002) than for their integration with monthly forcing ("MON"), with the former demonstrating higher rates of numerical mixing. We also note that GO5.0 does not apply any horizontal mixing, nor does it use the Gent and McWilliams (1990) scheme for parameterised adiabatic eddy mixing.

We present results from the final ten years (1996–2005) of the thirty-year model integration, and have used both the monthly mean output and the five-day output, the latter being expected to better represent the non-linear quadratic correlations.

3. The method

3.1. Using the watermass transformation framework to diagnose vertical mixing

Lee et al. (2002) derive, in their Appendix B, an expression for the effective diffusivity based on the watermass transformation framework of Walin (1982), which we shall not reproduce in full here. However, we will briefly summarise the method and define the quantities we will use to estimate the diapycnal fluxes and effective diffusivity. They define a watermass transformation streamfunction by adding the rate of change of the isopycnal volume in density space (which we will refer to as drift) to the overturning streamfunction:

$$G(\varphi, \rho) = \Psi(\varphi, \rho) + \frac{\partial}{\partial t} V(\varphi, \rho), \tag{1}$$

where ρ is the density and φ the latitude. Ψ(φ,ρ) is the overturning streamfunction, and V(φ,ρ) is the volume below the isopycnal surface ρ and south of φ. G(φ, ρ) is the net density transformation rate at the density surface (φ,ρ); this is primarily composed of the diffusive flux across the surface, but there are contributions from the non-linear equation of state (in this case cabbeling, since thermobaricity and neutral surface helicity are identically zero on a potential density surface), and from the convergence of density fluxes below the surface ρ. We assume both of these may be neglected in this analysis, but will discuss cabbeling in Section 4.

We define a diapycnal velocity g_{dia} as the diapycnal volume flux per unit area; this is related to G(φ,ρ) according to

$$\frac{\partial G(\varphi, \rho)}{\partial y} = \int_{x_W}^{x_E} g_{dia}\, dx \tag{2}$$

Assuming that there is no lateral diffusion of density below the isopycnal (we note that in the GO5.0 model configuration only the Redi isopycnal diffusion is used), and neglecting cabbeling, we may define the effective diffusivity as

$$\kappa_{eff} \approx \int_{\rho_{max}}^{\rho} \frac{\partial G(\varphi, \rho)}{\partial y} d\rho \Big/ \int_{x_W}^{x_E} \frac{\partial \rho}{\partial z} dx. \tag{3}$$

In this paper we shall also compare the diagnosed diapycnal velocity g_{dia} with the diapycnal velocity g_{diff} from the explicit mixing performed by the model:

$$g_{diff} = -\frac{\partial}{\partial \rho}\left(\kappa_{exp} \frac{\partial \rho}{\partial z}\right), \tag{4}$$

where κ_{exp} is the diffusivity prognosed by the mixing scheme.

The zonal mean upward diapycnal velocity $\langle g_{dia}(\varphi,\rho)\rangle$, where the angle braces imply zonal averaging, is derived from Eq. (2) by dividing the meridional divergence of the transformation streamfunction G(φ,ρ) by the zonal width across the basin of the density layer at latitude φ:

$$\langle g_{dia}(\varphi, \rho)\rangle = \frac{\partial G(\varphi, \rho)}{\partial y} \Big/ \int_{x_W}^{x_E} dx|_{\rho,y} \tag{5}$$

Substituting for G(φ,ρ) from Eq. (1) gives

$$\langle g_{dia}(\varphi, \rho)\rangle = \left[\frac{\partial \Psi(\varphi, \rho)}{\partial y} + \frac{\partial}{\partial t}\frac{\partial V(\varphi, \rho)}{\partial y}\right] \Big/ \int_{x_W}^{x_F} dx\Big|_{\rho,\varphi} - \left[\frac{\partial \Psi(\varphi, \rho)}{\partial y}\right] \Big/ \int_{x_W}^{x_F} dx|_{\rho,\varphi} + \frac{\partial}{\partial t}\langle z(\varphi, \rho)\rangle \tag{6}$$

where z(ρ) is the height of the isopycnal ρ in each water column, and where we define $\langle z(\varphi,\rho)\rangle$ as the zonal mean isopycnal height at latitude φ. We concern ourselves only with the interior part of the ocean that is not directly affected by surface forcing. We define a maximum surface density $\rho_{max}(\varphi)$ as a function of latitude as the maximum value, over the annual cycle, of the mean monthly surface density over the final ten-year period of the integration. We shall discuss here only those regions in density and latitude space (φ,ρ) where the density is higher than $\rho_{max}(\varphi)$; the Mediterranean and the Red Sea are excluded in the calculation of $\rho_{max}(\varphi)$, since their high surface densities ($\sigma_2 > 36.0\ \mathrm{kg\ m^{-3}}$) do not relate to direct surface influence on large-scale deep watermasses.

3.2. Numerical solution

The above equations were solved in the global, Atlantic and Indo-Pacific basins in latitude bands 2° wide, with the Atlantic and Indo-Pacific domains defined to extend from 35°S to 65°N. The vertical coordinate was chosen to be potential density, referenced to a pressure of 2000 dbar (σ_2): this quantity is conserved by construction in adiabatic processes, and this choice of reference pressure is accepted as a good compromise, maintaining monotonicity in near-surface waters and in the abyss over most of the ocean. 72 density classes were used (values listed in Table 1), spanning the range $30.0 < \sigma_2 < 37.2\ \mathrm{kg\ m^{-3}}$: a linear density scale was used for $\sigma_2 < 35.0\ \mathrm{kg\ m^{-3}}$, while a logarithmic mapping onto the axis was used at densities higher than $35.0\ \mathrm{kg\ m^{-3}}$ in order to have a good representation of deep and bottom waters. In evaluating the diapycnal fluxes, a three-point smoother was applied in the vertical to reduce sampling effects in the conversion from depth to density coordinate. The overturning transports and the zonal integrals were first evaluated on model grid rows for consistency, and then assigned to latitude bins.

For exact results, transports should be assigned to density classes at each timestep during integration and a running time average carried

Table 1
Density classes used in analysis.

Index	Lower σ_2 bound	Index	Lower σ_2 bound	Index	Lower σ_2 bound
1	0.0000	25	35.97566	49	36.74813
2	30.00000	26	36.02115	50	36.77111
3	30.55556	27	36.06487	51	36.79363
4	31.11111	28	36.10692	52	36.81570
5	31.66667	29	36.14746	53	36.83733
6	32.22222	30	36.18656	54	36.85857
7	32.77778	31	36.22434	55	36.87940
8	33.33333	32	36.26089	56	36.89985
9	33.88889	33	36.29626	57	36.91993
10	34.44444	34	36.33056	58	36.93965
11	35.00000	35	36.36383	59	36.95904
12	35.10622	36	36.39613	60	36.97808
13	35.20319	37	36.42753	61	36.99682
14	35.29239	38	36.45806	62	37.01524
15	35.37498	39	36.48778	63	37.03336
18	35.45187	40	36.51674	64	37.05119
17	35.52380	41	36.54495	65	37.06874
18	35.59136	42	36.57246	66	37.08602
19	35.65506	43	36.59932	67	37.10303
20	35.71531	44	36.62555	68	37.11979
21	35.77247	45	36.65117	69	37.13630
22	35.82685	46	36.67621	70	37.15257
23	35.87869	47	36.70071	71	37.16861
24	35.92823	48	36.72467	72	37.18441

out of these in density space. However, since this framework is not included in the NEMO v3.4 code, we use the time averages that are available from the model integration to derive an acceptable approximate solution. The transformation streamfunction and the effective diffusivity were calculated from both monthly and 5-day mean outputs from the last ten years of the GO5.0 model integration. It was found that, although the overall form of the results was rather similar with the two averaging periods, the streamfunction was smoother with the higher-frequency forcing, so the results we present here are from the 5-day means. The drift terms were evaluated from the difference in the mean isopycnal heights $z(\rho)$ averaged over 5-day means in the first and last years of the ten-year period.

We shall present zonally averaged values of diffusivity – both explicit and diagnosed – in density classes. The diffusivity in these averages is weighted by the vertical density gradient, since this corresponds to a diapycnal or vertical density flux, rather than a simple thickness-weighted mean.

4. Results

4.1. The overturning streamfunction and watermass transformations

The overturning streamfunction, calculated with potential density as the vertical axis, allows a qualitative visualisation of the large-scale effects of diapycnal mixing, as it explicitly shows the transport of water across density surfaces. Fig. 1 shows the streamfunctions in the global, Atlantic and Indo-Pacific domains, evaluated as a function of potential density, averaged over the final ten years of the GO5.0 integration. In the steady state, non-horizontal streamlines imply density transformations. The poleward surface circulation (labelled here by green arrows) is generally associated with buoyancy loss to the atmosphere, which corresponds to streamfunction contours that slope downward in density space along the direction of flow. In the interior, unventilated circulation is generally along streamlines that slope upwards towards lower densities, corresponding to buoyancy gain of dense waters due to downgradient mixing with overlying light water, although the downward-inclined streamlines below $\sigma_2 = 37.0$ at the base of the southward-flowing NADW in the Atlantic also correspond to mixing, in this case with the underlying denser AABW. The absence of negative contours in the abyss in Fig. 1(b) implies that the flow of Antarctic Bottom Water into the Atlantic has ceased after twenty years of integration, although Fig. 1(c) shows that over 12 Sv of AABW is still upwelling in the Indo-Pacific, where it forms the dominant overturning cell.

It is clear in Fig. 1 that not all the interior streamlines are monotonic: in particular, there is a "bulge" in the global circulation between 40° and 55°S at densities between 36.2 and 37.0, as well as apparently closed cells in the AABW circulation. We shall show that these instances are partly due to adjustment processes related to slow model drift, and the residual is likely to result chiefly from nonlinearities in the equation of state. Cross-correlations between density and mass transport on timescales shorter than the 5-day averaging period used here are also likely to form some contribution; using 5-day means leads to rather smoother streamlines and diapycnal velocity fields than those derived from monthly means and, while there is no reason to assume that shorter time averages would not lead to further improvements, these were not available.

4.2. Diapycnal velocities from the model's mixing scheme

Fig. 2(a) shows the mean tracer diffusivity κ on a logarithmic scale

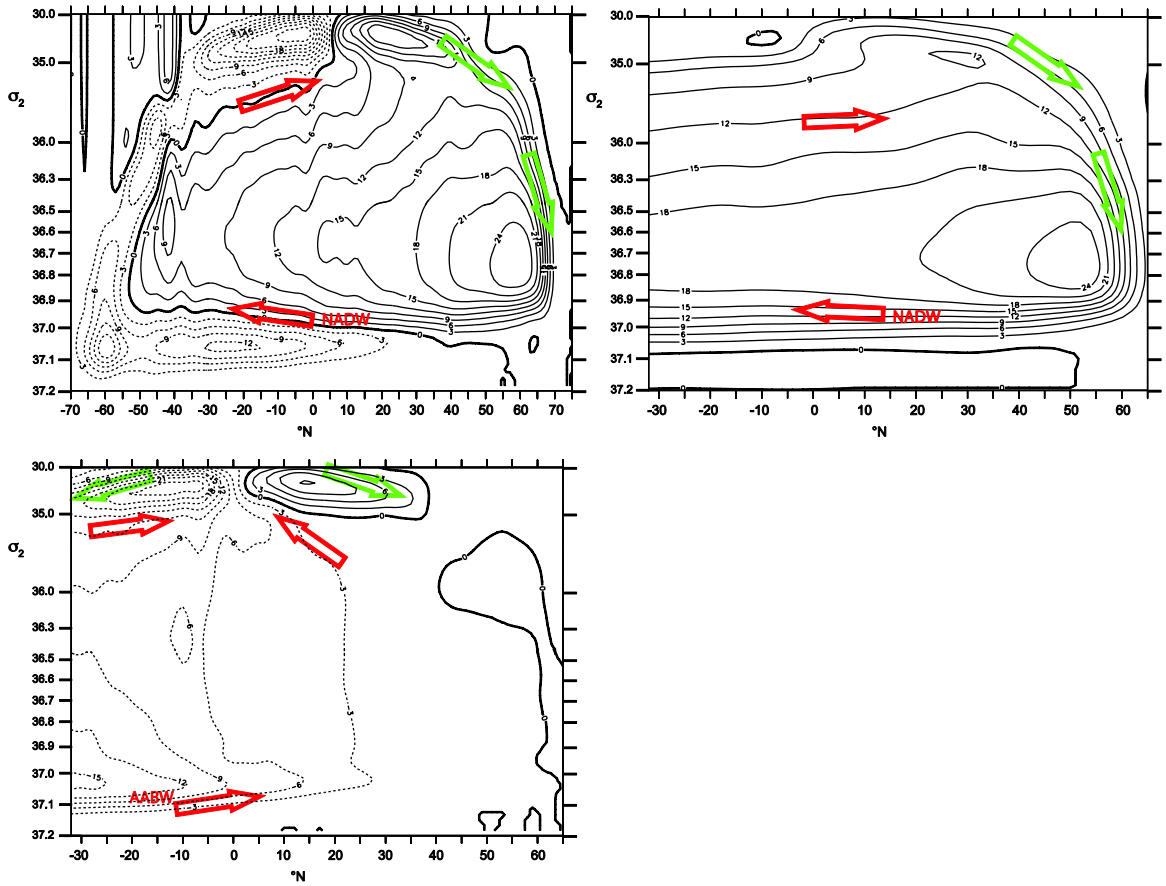

Fig. 1. (a) Global, (b) Atlantic and (c) Indo-Pacific streamfunctions as functions of latitude and potential density σ_2, calculated from 5-day means over the final ten years of the GO5.0 integration: dashed contours correspond to negative values. The arrows show the sense of the overturning circulation: green denotes surface-forced water transformation, and red arrows interior transformations. (For interpretation of the references to color in this figure legend, the reader is referred to the web version of this article.)

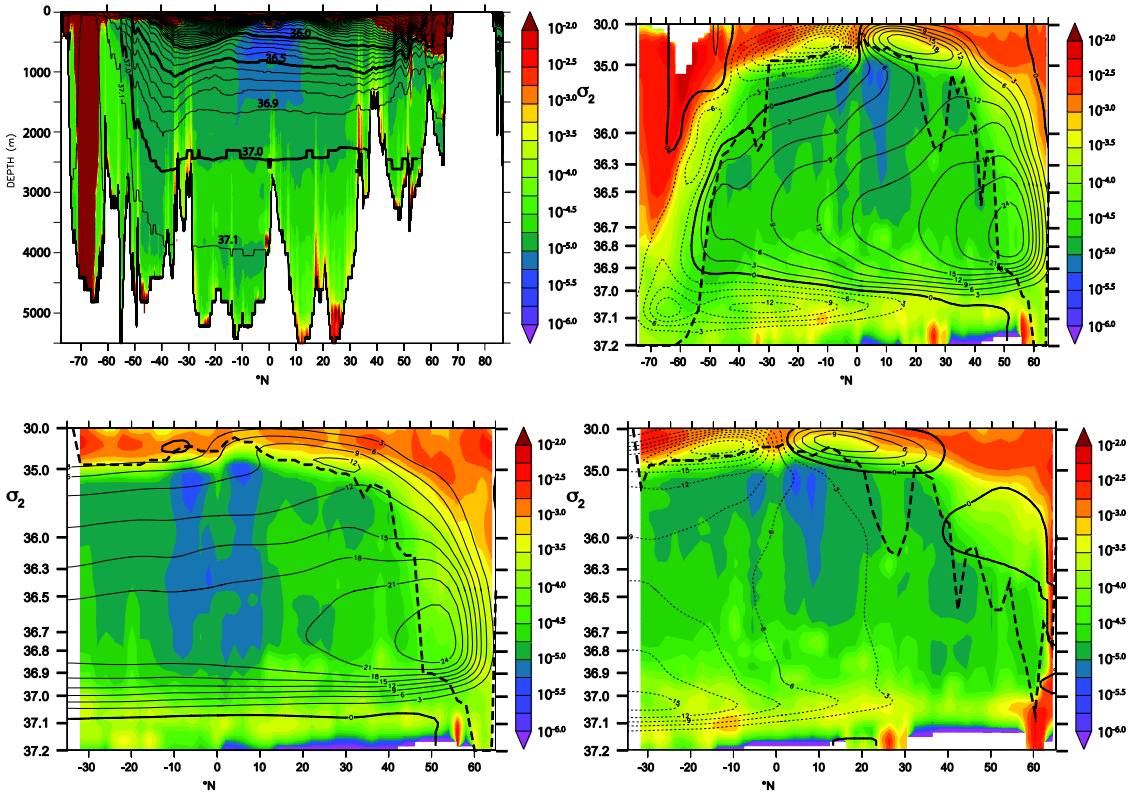

Fig. 2. The mean tracer diffusivity κ_{exp} in $m^2\,s^{-1}$ on a logarithmic scale: (a) diagnosed from the TKE mixing scheme in GO5.0 as a function of depth on a section at 30°W; and evaluated in density classes in (b) the global domain; (c) in the Atlantic; and (d) in the Indo-Pacific.

as a function of depth, as calculated by the TKE scheme in GO5.0, averaged over the final ten years of the integration on a section at 30°W, with contours of the potential density σ_2. The $\sigma_2 = 37.1$ contour approximately marks the upper boundary of Antarctic Bottom Water (AABW), with North Atlantic Deep Water (NADW) overlying it. This shows that the TKE mixing scheme used by the model enhances the mixing coefficient over the mid-ocean ridges, but, away from the ridges, the mixed layer, and the high-latitude convection regions, the explicit diffusivity generally takes values between the background diffusivity (between 1.2×10^{-6} $m^2 s^{-1}$ within 5° of the Equator and 1.2×10^{-5} $m^2 s^{-1}$ in the extra-tropics) and around ten times the background value, generally increasing downwards. The large diffusivities at the southern end of the section correspond to the Weddell Polynya and the associated deep convection that develop in the third decade of the model integration, as described in Megann et al. (2014).

Fig. 2(b) shows the same field as in (a), but now evaluated in density classes in the global domain, along with the overturning streamlines (solid and dashed lines) and an indication of the maximum annual surface density (bold dashed line). Again, the large values in the surface-forced boundary layer are clear, as is the reduced diffusivity close to the Equator. In the interior, the diffusivity tends to increase with density, being generally less than 2×10^{-5} $m^2\,s^{-1}$ at densities less than 36.5 kg m^{-3}, but exceeding 1×10^{-4} $m^2\,s^{-1}$ at densities greater than 37.0 kg m^{-3}. Comparison with Fig. 2(a) shows that the latter enhanced values correspond to Antarctic Bottom Water or to watermasses lying directly above AABW. Fig. 2(c) and (d) shows the diffusivity in density classes in the Atlantic and Indo-Pacific, respectively: the dependence of the diffusivity on latitude and density is similar to that in the global domain.

We note that overall the values of κ used by the model are not inconsistent with the diffusivity profiles published by Kunze et al. (2006) and by Waterhouse et al. (2014), derived from a wide selection of microstructure measurements. Specifically, these authors infer values of between 10^{-6} and 10^{-5} $m^2\,s^{-1}$ in the ocean interior, with enhanced values of between 10^{-6} and 10^{-5} $m^2\,s^{-1}$ above rough topography.

As a baseline for comparison with the effective mixing in the model, we first evaluate the diapycnal velocities produced by the explicit mixing scheme in the model g_{diff}, as defined in Eq. (4). These are presented as a function of latitude and density (Fig. 3(a)) and as a global plot on three density surfaces (indicated by the horizontal dashed red lines in Fig. 3(a)): firstly $\sigma_2 = 36.70$ (Fig. 3(b)) corresponds to a surface just above the southward flowing deep waters; $\sigma_2 = 36.91$ (Fig. 3(c)) is in the centre of the southward-flowing NADW; and $\sigma_2 = 37.07$ (Fig. 3(d)), which lies close to the upper boundary of Antarctic Bottom Water. Values of g_{diff} in the interior region (densities below the dashed black line, corresponding to the maximum annual surface density) are generally positive, consistent with down-gradient diapycnal flow. The values generally increase from the abyss to the deep and intermediate waters, consistent with the increasing magnitude of the vertical density gradient, and are high (above 5×10^{-7} m s^{-1}) in the mixed layer. The alternating sign of the diapycnal velocity seen between 10°S and the Equator in Fig. 3(a) is a numerical artefact from discretisation. The negative values in the abyss are a combination of the sharp bottom-intensification of the diffusivity from the TKE scheme ($\partial\kappa/\partial z$ reverses sign near the bottom, as is clearly shown in Fig. 2), along with the relatively coarse resolution when the fields are projected into density space. Typical values at the top of the deep waters ($\sigma_2 = 36.70$) are around $+0.5 \times 10^{-7}$ m s^{-1}, or approximately 1.5 m/year.

Fig. 4 shows the rate of change of the height of isopycnal surfaces z (ρ) in the global ocean as a function of latitude and density, as well as zonally averaged on the same density surfaces as Fig. 3. Positive values imply an increase in density at a given depth in the water column over time. Over much of the global ocean, the two lighter isopycnals are deepening, corresponding to a lightening of watermasses, with the highest rate of drift (up to 2×10^{-7} m s^{-1}, or around 6.5 m/year) seen in the Southern Ocean and in the Atlantic north of about 30°N: this can be interpreted as a general replacement of denser watermasses by lighter water, thereby depressing the isopycnals. The rate of isopycnal

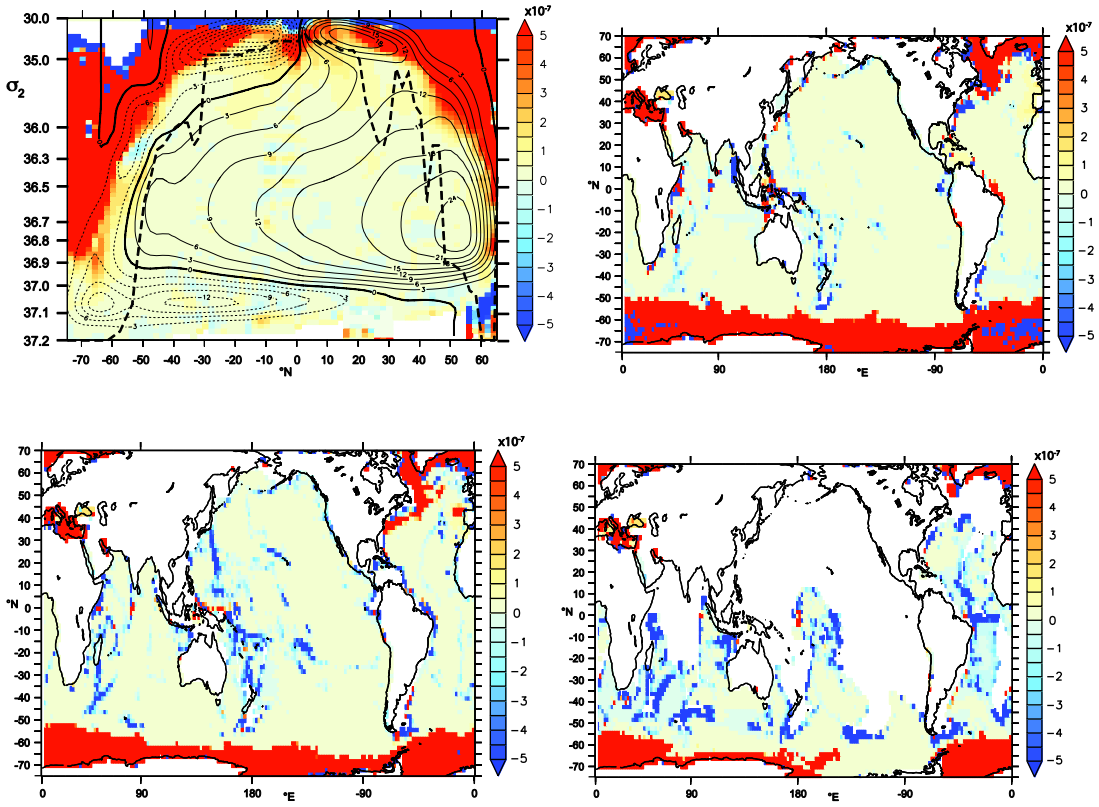

Fig. 3. Diapycnal velocity ($\times\ 10^{-7}$ m s^{-1}) from explicit mixing: (a) zonal means in the global domain; and on the potential density surfaces (b) $\sigma_2 = 36.70$; (c) $\sigma_2 = 36.91$; and (d) $\sigma_2 = 37.07$, from 5-day means over the final ten years of the GO5.0 integration.

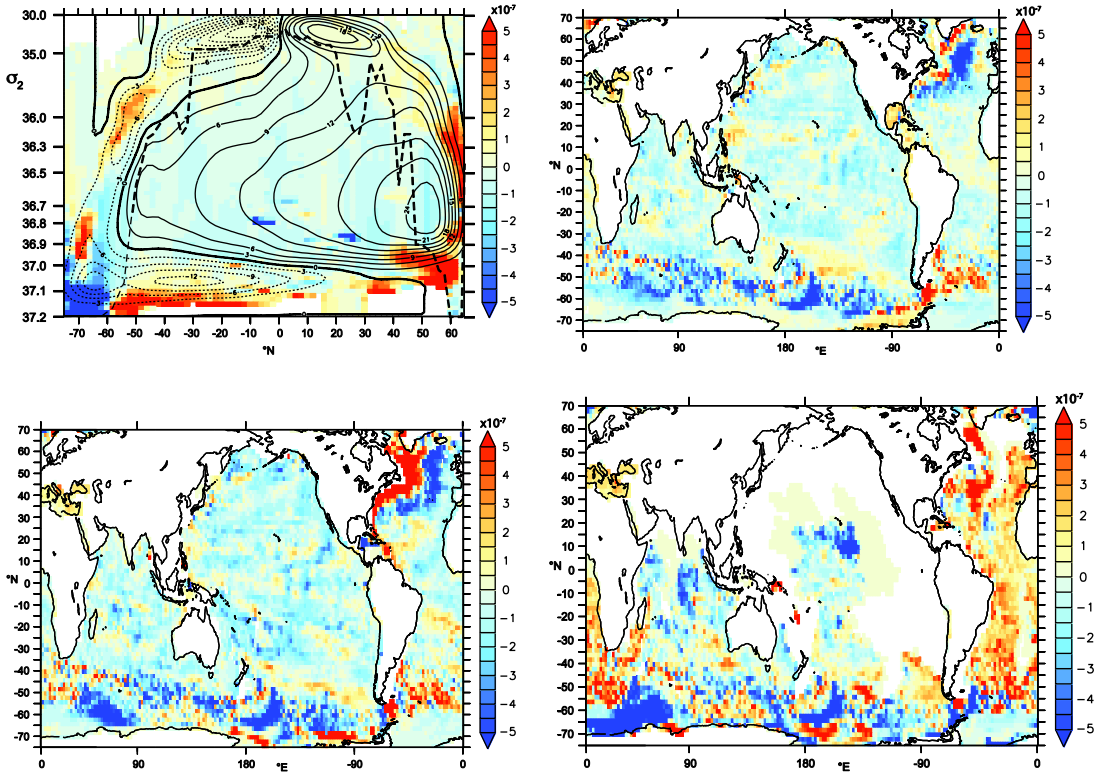

Fig. 4. Rate of change of height of isopycnals ($\times\ 10^{-7}$ m s^{-1}): (a) zonal means in the global domain; and on the potential density surfaces (b) $\sigma_2 = 36.70$; (c) $\sigma_2 = 36.91$; and (d) $\sigma_2 = 37.07$, from 5-day means over the final ten years of the GO5.0 integration.

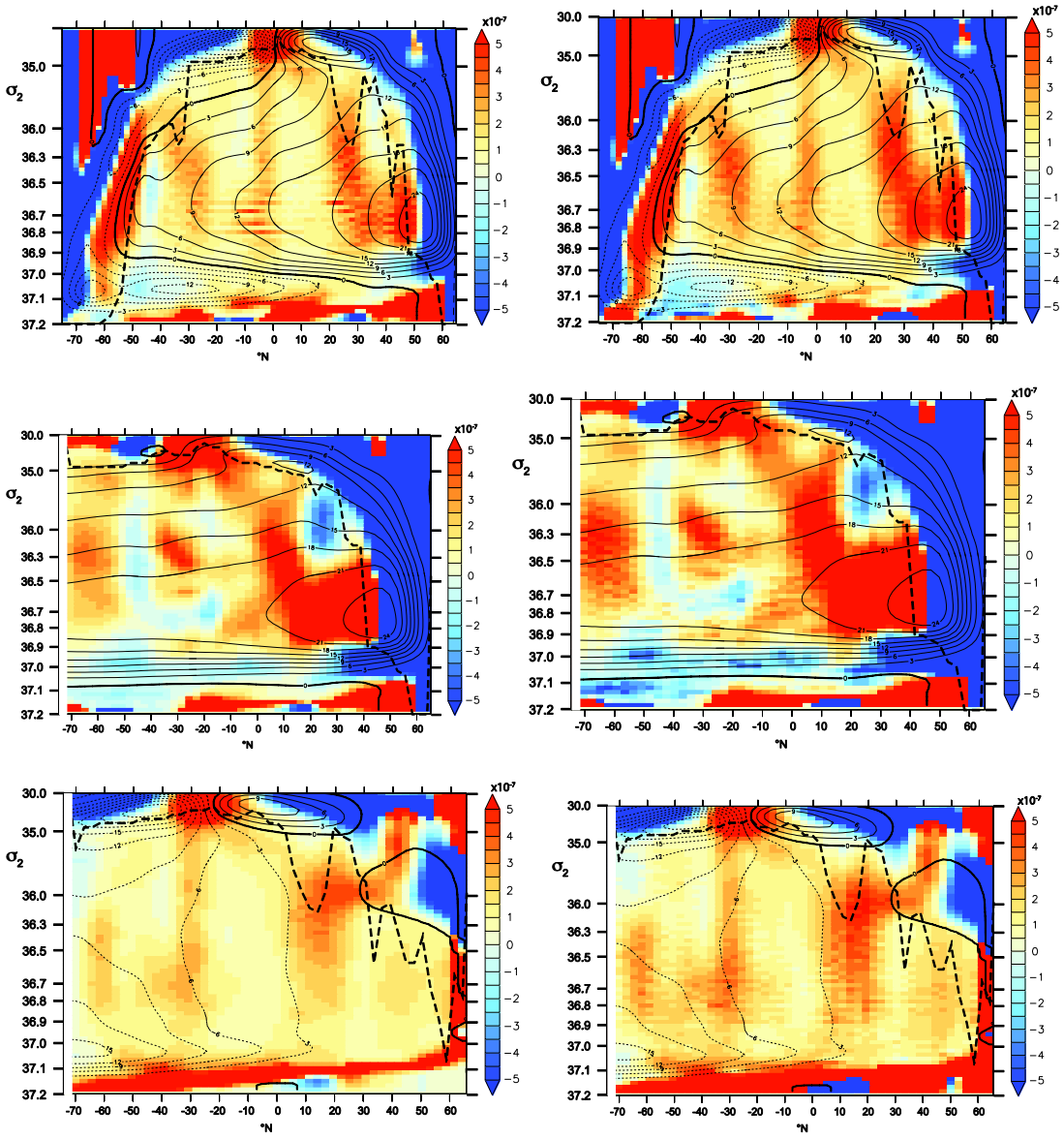

Fig. 5. Upward diapycnal velocity ($\times 10^{-7}$ m s^{-1}) from 5-day means over the final ten years of the GO5.0 integration derived from: (a) the divergence of the streamfunction in the global domain; (b) the sum of divergence and drift in the global domain; (c) the divergence of the streamfunction in the Atlantic; (d) the sum of divergence and drift in the Atlantic; (e) the divergence of the streamfunction in the Indo-Pacific; and (f) the sum of divergence and drift in the Indo-Pacific.

displacement is generally large compared with the fluxes due to explicit mixing, but is less spatially smooth than the latter, especially away from the Equator. The densest isopycnal ($\sigma_2 = 37.07$) shows a contrast between the Atlantic and the rest of the world ocean, indicating a reduction of the volume of the bottom waters in the Atlantic and an increase elsewhere; this is consistent with the presence of a strong AABW cell in the Indo-Pacific and the near-disappearance of this cell in the Atlantic (Fig. 1).

4.3. Diagnosed diapycnal velocities

We now evaluate the diagnosed diapycnal velocities defined in Eq. (5) for comparison with the diapycnal velocity g_{diff} associated with the explicit mixing parameterised by the model, as defined in Eq. (4). We expect these to be a sum of the transformation rate resulting from the explicit mixing and a term resulting from the numerical mixing in the model, which is likely to be generally (but not necessarily) positive. In Fig. 5 we show the diapycnal velocity estimated from the streamfunction alone g_{ψ} and the total g_{dia} as functions of density and latitude in the global domain, with the overturning streamfunction again overlain to indicate the circulation in density space, and with the minimum monthly-mean surface density plotted (bold dashed line) to delimit the directly surface-forced transformation regime. Away from the surface-forced mixed layers, the diapycnal velocity associated with advection across isopycnals g_{ψ} is mainly positive, corresponding to transformation toward lower densities, with typical velocities of between 1×10^{-7} and 4×10^{-7} m s^{-1}, or 3–12 m/year. Higher values are seen north of 40°N and south of 40°S, as well as in the equatorial upwelling regions; we note that these relatively high transformation rates lie in locations in density and latitude space that are at least partially surface forced. Including the drift term generally has two effects: increasing the diagnosed rate of transformation to lower densities, and acting to cancel some of the downward diapycnal velocities, for instance at $\sigma_2 = 36.6$ and between 40° and 50°S (see Fig. 5(b)) and in the North Atlantic between 35°N and 40°N above $\sigma_2 = 36.0$ (Fig. 5(d)). There remain regions with a negative g_{dia}, in particular in the Southern Ocean between 50° and 40°S, in the abyssal Atlantic below $\sigma_2 = 36.9$ and at intermediate densities in the tropical Atlantic. In the latter case, the negative

diapycnal velocities correspond to downward kinks in the streamlines in both the southward-flowing NADW and in the intermediate water flowing northward above it: these kinks seem to be robust, also appearing when the streamfunction is calculated with reference pressure of 1000 dbar and 0 dbar, as well as being independent of the numerical package used to evaluate Ψ.

Comparison of the diagnosed diapycnal velocity g_{dia} (Fig. 5(b)) with the zonal mean diapycnal velocity g_{diff} from explicit mixing (Fig. 3(a)) reveals that, while the latter is between -0.5 and $+1.5 \times 10^{-7}$ m s^{-1} everywhere within the non-surface-forced regime, with negative values close to the Equator and at the upper boundary of AABW, g_{dia} is positive almost everywhere outside the Southern Ocean, and in certain latitude bands exceeds $+5 \times 10^{-7}$ m s^{-1}. Although the enhanced g_{dia} in the model does not by itself imply high rates of numerical mixing, we shall show in Section 4.4 that the effective diffusivity derived from g_{dia} is substantially larger than the explicit diffusivity.

A question that is pertinent at this point is whether the large values of the diapycnal velocities derived from the overturning streamfunction are an artefact of carrying out the analysis in potential density space, rather than using the locally-referenced density surfaces used in the model advection and mixing schemes (clearly a streamfunction cannot be meaningfully defined on the latter surface, which is non-conservative). As we have already shown, the diagnosed diapycnal velocities are large compared with those expected from the model mixing scheme in the potential density range $35.5 < \sigma_2 < 36.9$ (e.g. Fig. 5(a)), which, as can be verified by inspection of Fig. 2(a), corresponds roughly at mid-latitudes to depths between 2000 and 500 m. Over this depth range our choice of 2000 dbar as reference pressure P_{ref} for the density coordinate may not be optimal. To investigate the sensitivity of our results to the particular choice of P_{ref}, the streamfunction was evaluated in the final year of integration for both $P_{ref} = 1000$ and 2000 dbar, and the zonal mean global diapycnal velocity g_{Ψ} derived from this in each case, with the overturning streamlines drawn as contours for reference (Fig. 6). It should be noted that the range of values in Fig. 6 is reduced relative to that used in Fig. 5 for clarity, while the values of σ_1 for the vertical scale are chosen to represent the overturning cells in the two cases as comparably as possible. If the high transformation rates already described were mainly due to the use of an inappropriate reference pressure, we would expect the diapycnal velocity at depths between 500 and 1500 m to be substantially reduced when the reference pressure is changed from 2000 dbar to 1000 dbar. Instead, the zonal mean of g_{Ψ} has similar magnitudes in the two cases, with close correspondence between the regions of larger transformation rates in subtropical latitudes as well as between those regions where g_{Ψ} is close to zero are even negative, namely in the Southern Ocean and between 0° and 10°N. There is, nevertheless, some sensitivity to reference pressure: the values where the NADW flows southwards in the southern hemisphere at 1500–2000 m depth are 30–40% larger with σ_1 (Fig. 6(a)) than with σ_2 (Fig. 6(b)), although little corresponding increase in g_{Ψ} is seen with σ_2 at lower densities (i.e. shallower depths). All the same, we may conclude with some degree of confidence that our results are to first order robust to the choice of coordinate system used.

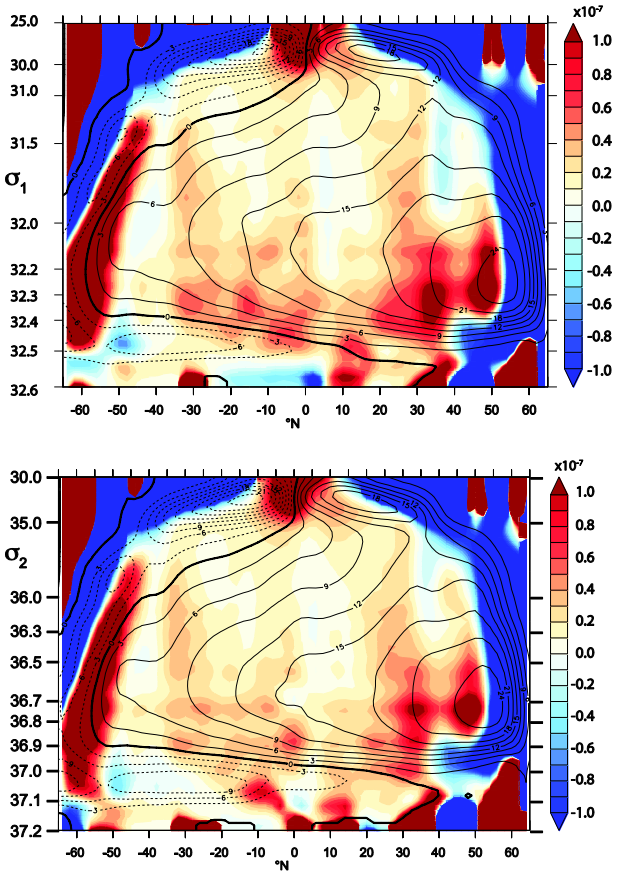

Fig. 6. Upward diapycnal velocity ($\times 10^{-7}$ m s^{-1}) from 5-day means over the final year of the GO5.0 integration, derived from the divergence of the streamfunction in the global domain using potential density defined with reference pressure (a) 1000 dbar and (b) reference pressure 2000 dbar.

4.4. Estimation of the diapycnal diffusivity

In this section we compare the diapycnal diffusivities diagnosed from Eq. (3) with the explicit diffusivity in the model. If our method correctly expresses the watermass transformation rate from the total mixing performed by the model, the value of diffusivity it gives will be equivalent to the explicit diffusivity plus an increment due to numerical mixing; as shown in Section 4.3, the diapycnal velocity is generally between 2 and 10 times larger than that implied by the explicit diffusivity and the local density gradient, so we might expect the effective diffusivity to be proportionally larger than the diffusivity applied by the model. Fig. 7 shows the effective diffusivity κ_{eff} on the same logarithmic scale as Fig. 2 in the last ten years of GO5.0 in the global, Atlantic and Indo-Pacific domains, evaluated as in Eq. (3) from the divergence of the overturning streamfunction and the rate of isopycnal drift. In each case, contours of the overturning streamfunction are overlain to show the mean circulation and, as before, the maximum monthly surface density is denoted by a bold dashed line. The white areas show negative diffusivities. On comparison with Fig. 2, it is immediately clear that the diffusivity inferred from the watermass transformation rate is substantially larger than the explicit diffusivity over much of the ocean at densities higher that the surface-forced region. In the global domain (Fig 6(a)), the region of low diffusivity of below 10^{-5} m^2 s^{-1}, between the Equator and 10°N and for densities between the base of the mixed layer and $\sigma_2 = 36.3$, is correctly diagnosed by our scheme, indicating that the numerical mixing is low here; similarly, the diagnosed diffusivity also shows the reduction in value around the Equator in all ocean basins (the negative value at $\sigma_2 \approx 36.3$ at 5°N in the Indo-Pacific is close to zero, and is likely to result from a truncation error). In the densest layers ($\sigma_2 > 37.0$) the mixing appears to be dominated by the parameterised enhancement of mixing over rough topography, since the values of κ_{eff} and κ are comparable here. Elsewhere, however, there are values of 3×10^{-4} m^2 s^{-1} in the density range between $\sigma_2 = 36.0$ and $\sigma_2 = 36.9$ at all latitudes, compared with the model diffusivity which is generally between 3×10^{-5} and 1×10^{-4} for these watermasses.

The three regions in Fig. 7 where there are significant negative diagnosed diffusivities in the ocean interior merit comment. These comprise the latitude range 40°−50°S in the Southern Ocean; two patches in the North Atlantic between 30°N and 50°N; and lastly in the tropical Atlantic between 20°S and 5°S. The former two regions correspond quite closely to the regions where Klocker and McDougall (2010)

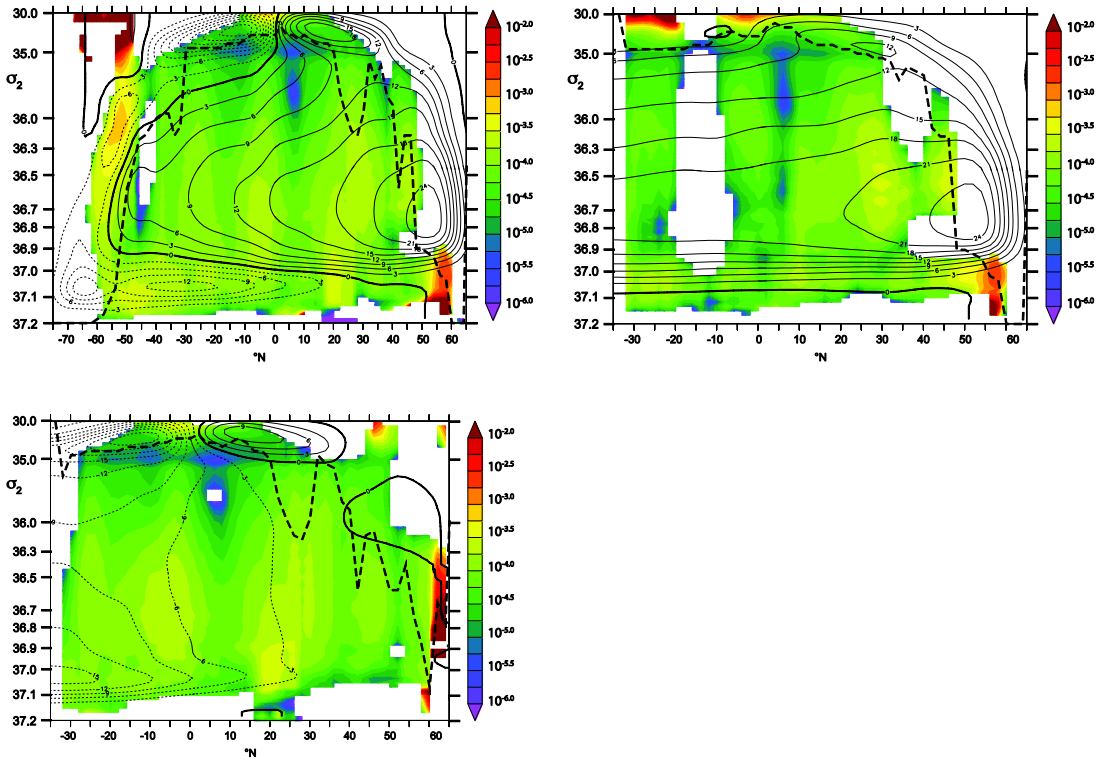

Fig. 7. (a) The effective diffusivity κ_{eff} in $m^2\ s^{-1}$ on a logarithmic scale in the last ten years of GO5.0, diagnosed from the watermass transformation rate: (a) in the global domain; (b) in the Atlantic, and (c) in the Indo-Pacific.

calculated substantial "antidiffusive" watermass transformation rates arising from the nonlinear equation of state (mainly cabbeling and thermobaricity) in a coarse resolution model; these authors estimated diapycnal velocities of around 10^{-7} m s^{-1}, which are not inconsistent with the values of 0.5–1.0 × 10^{-7} m s^{-1} in Fig. 5(a). Meaningful off-line calculation of the transformation rates from these processes in an eddying model such as GO5.0 is near-impossible, but it seems reasonable to ascribe the negative diffusivities in these first two regimes to nonlinearities in the equation of state. The negative values in the tropical Atlantic, however, are unlikely to arise from this source, and probably result from shortcomings in the analysis, possibly from the neglect of eddy terms in the calculation of volume transports, which are noted by Nurser and Lee (2004) to give rise to spurious features in the overturning circulation. We note that the circulation at the western boundary of the Atlantic between the Equator and 20°S in this model is particularly complex, with the southward Deep Western Boundary Current partly overlapping in depth with the northward Brazil Current; with each carrying around 10 Sv, small truncation errors in the partition of the transport into density classes may plausibly lead to the non-monotonicity of streamlines seen here.

Finally, to clarify the relative contributions of numerical and physical mixing in the model, Fig. 8 shows the ratios of the diagnosed diffusivity (Fig. 7) to the explicit diffusivity (Fig. 2) as a function of latitude and density in the global, Atlantic and Indo-Pacific regions. If the numerical mixing is negligible, the ratio should approach unity, while if numerical mixing is significant, the ratio will be appreciably larger than unity. In the global domain, the ratio is greater than unity almost everywhere below the maximum surface density; the exceptions are the region of negative diagnosed diffusivity between 40° and 50°S already mentioned, and in the abyssal waters with potential densities greater than 37.1 kg m^{-3} (although there are enhanced diffusivity values of up to 5 times the explicit value in the northward flowing Antarctic Bottom Water south of 40°S). This confirms our interpretation of Fig. 7: namely, that in the deep waters and intermediate waters the numerical mixing is up to an order of magnitude larger than the mixing performed by the mixing scheme.

4.5. Comparisons with Lee et al. (2002) results

Lee et al. (2002) estimated the rate of isopycnal drift, the diapycnal velocity and the effective diffusivity in the southern hemisphere for the 0.25° global OCCAM model, which may be directly compared with the results we have obtained for GO5.0. We note that our 20-year spin-up of the model before diagnostics are calculated is more than twice the length as the 8 years used by Lee et al. (2002), so we might expect the diapycnal velocities due to model drift to be smaller, relative to those from mixing, than in the results presented in the latter paper. Indeed, where the AABW cell in the OCCAM model appeared to have shut down during the spinup period, GO5.0 produces 12 Sv of AABW and is able to export at least a part of this into the northern hemisphere. Qualitatively, Lee et al. found isopycnals to be sinking at around 5 m/year south of 35°S; while in GO5.0 (Fig. 4(a)) the isopycnals are sinking at between 1.5 and 4.5 m/year in the Southern Ocean.

The diapycnal velocities in the region of the path of the Antarctic Circumpolar Current (ACC) in OCCAM (Lee et al.'s Fig. 7(a)) were estimated to be 40 m/year or more, corresponding to a total water mass transformation rate of around 15 Sv between 40°S and 60°S. The transformation rate in GO5.0 may be estimated from Fig. 5; there is about 12 Sv of upwelling in this latitude range (Fig. 5(a)), and when the drift term is taken into account (Fig. 5(b)) the total transformation rate is likely to be comparable to that in OCCAM. The effective diapycnal diffusivity in the OCCAM run with six-hourly winds (Fig. 8(c) in Lee et al.) has values of over $10^{-4}\,m^{-2}\ s^{-2}$ in the density range $36.84 < \sigma_2 < 36.94$ everywhere south of the Equator, increasing to 5–10 × $10^{-4}\,m^{-2}s^{-2}$ south of 50°S, with patches of negative diffusivities $36.70 < \sigma_2 < 36.80$ between 35°S and the equator. In GO5.0 (Fig. 7(a)), κ_{eff} is greater than $10^{-4}\ m^2\ s^{-1}$ in densities between 36.50 and 37.10, with enhanced values south of 50°S, and the negative values extend over a similar density range as that in OCCAM, but are limited to the latitude band 50°S–40°S. In summary, our results are quantitatively

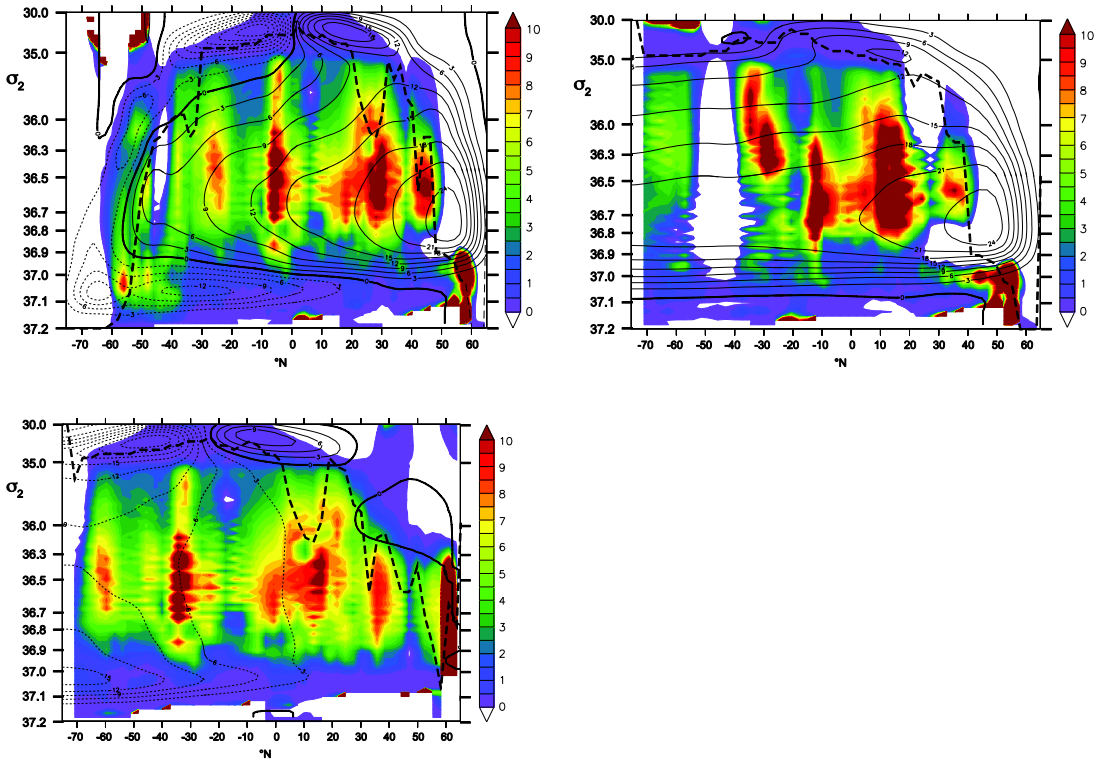

Fig. 8. The ratios of the diagnosed diffusivity to the explicit diffusivity as a function of latitude and density: (a) in the global domain; (b) in the Atlantic; and (c) in the Indo-Pacific. White areas show negative ratios.

consistent with those of Lee et al.

5. Sources of numerical mixing

5.1. Characterisation of transient flows

The main source of numerical diapycnal mixing in the ocean interior is from truncations in the advection scheme where flow is across isopycnals, either by transient motions or by the mean circulation. As noted by Griffies et al. (2000), numerical mixing of tracers results from the irreversible component of the numerical advection, which is some, ideally negligibly small, fraction of the physical, reversible advection of which the advection scheme is an approximate representation. In this section we characterise the vertical motions in the model and discuss their relationship to the numerical diffusivity in the GO5.0 model.

The types of mesoscale variability found in a numerical ocean model of this resolution may be characterised as follows: firstly the coherent wavelike features in the upper 1000 m of the tropical Atlantic and Pacific usually referred to as Tropical Instability Waves (Legeckis, 1977) with dominant wavelengths of around 1000 km, but with highly filamentary structure within this; eddy-like mesoscale variability with a length scale around the first baroclinic Rossby radius, associated with strong currents such as separated western boundary currents and the Antarctic Circumpolar Current; near-inertial gravity waves energised by wind stress variability at the western boundary (e.g. Blaker et al, 2012); internal waves and tides; and finally noise-like features at or close to the grid scale, where the grid is unable to resolve the eddy-like features created by barotropic or baroclinic instability (mainly at high latitudes and on coastal shelves). All of these have strong transient vertical velocities of a metre per day or more; in the ocean this motion generally takes the form of isopycnal heave, which in non-breaking cases results in negligible mixing, but in depth-coordinate models produces significant cross-coordinate flow and therefore has the potential to create numerical mixing.

In Fig. 9 we show the mean and RMS vertical velocities from a ten-year average of 5-day means, on the same potential density surfaces as in Fig. 2. The mean vertical velocities in the gyre-scale upwelling and downwelling regions are typically less than 2×10^{-7} m s^{-1}, or 10–20 cm/day, while the upwelling rate in the Southern Ocean is around twice this. There are vertical velocities of up to 10–20 $\times 10^{-7}$ m s^{-1} with sign alternating over a hundred kilometres or so along the path of the ACC and separated boundary currents. The RMS velocities, by contrast, reach ten to a hundred times the mean in eddy-rich regions such as the Southern Ocean and the North Atlantic. The eddy-like features in the vertical velocity field are found to be well correlated vertically over two or three thousand metres depth, and examination of their time evolution reveals that they are mainly advected by the mean circulation, or propagate independently, rather than being stationary. We note that the RMS vertical velocities in a 5-day mean output file in these regions are typically ± 5 m/day, and we shall show in Section 5.3 that instantaneous vertical velocities are significantly larger than this. We conclude that there are persistent vertical motions over most of the ocean depth that have at least the potential to cause significant numerical mixing.

5.2. Relation between and transient vertical motions and numerical mixing

In a pure isopycnic model, where the coordinate surfaces in any water column rise and fall in response to vertical adiabatic motions, the passage of wavelike or eddy-like features will not lead to numerical mixing. In a model with a fixed vertical coordinate, by contrast, vertical motions will inevitably cause advection across the coordinate surfaces if there is a vertical gradient of a tracer, and hence will cause at least some mixing, even in the absence of explicit mixing. The rate of change of density due to vertical advection is given by

$$\frac{\partial \rho}{\partial t} = w \frac{\partial \rho}{\partial z}. \tag{7}$$

If the vertical velocity w consists primarily of an alternating flow with a relatively small mean value, it is more useful in this context to

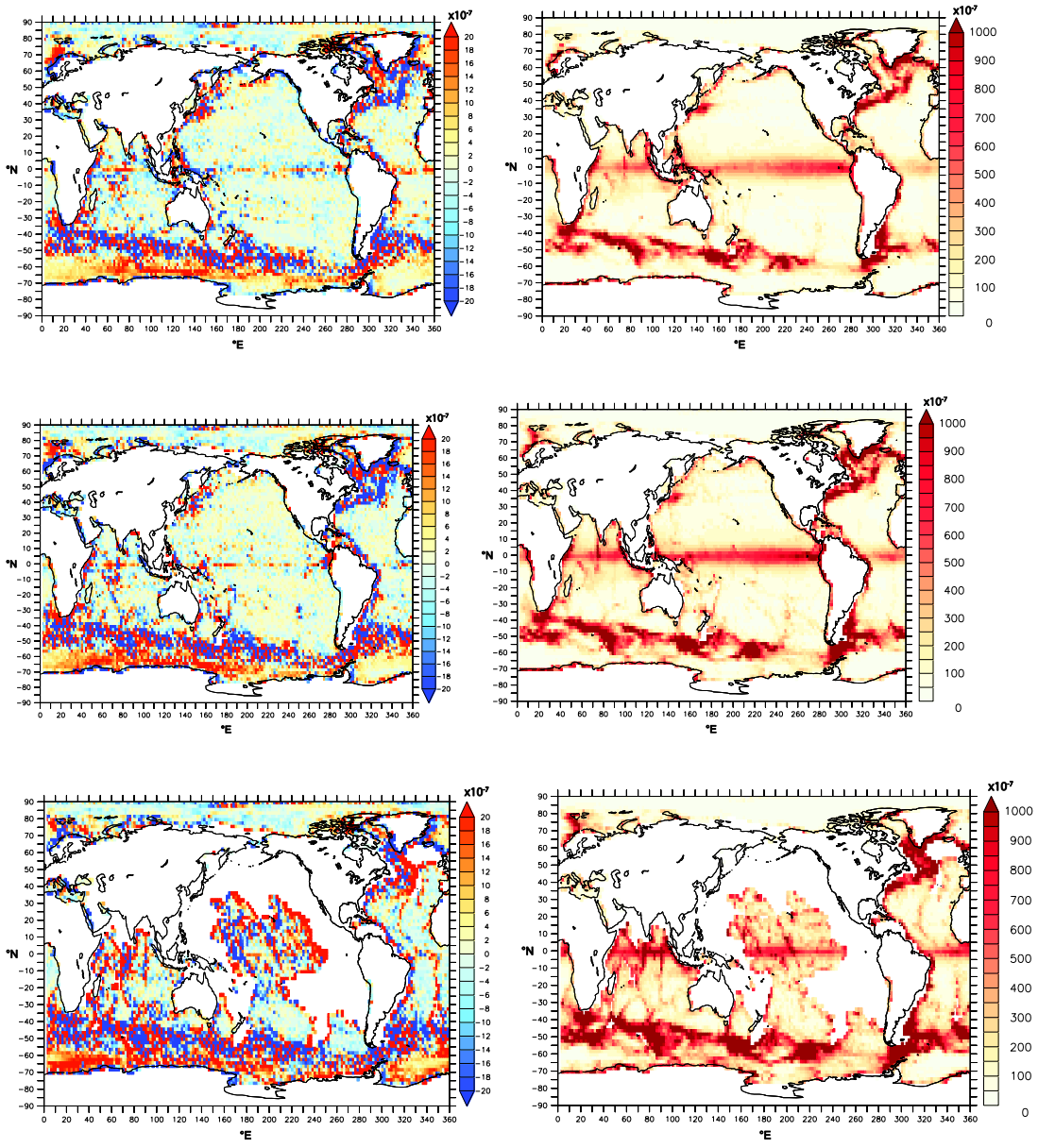

Fig. 9. (a) The mean vertical velocity ($\times 10^{-7}$ m s^{-1}) and (b) the standard deviation of vertical velocity on the potential density surface $\sigma_2 = 36.70$; (c) the mean vertical velocity and (d) its standard deviation on surface (c) $\sigma_2 = 36.91$; (e) the mean vertical velocity and (f) its standard deviation on surface $\sigma_2 = 37.07$, from 5-day means over the final ten years of the GO5.0 integration.

consider the standard deviation of the advection:

$$\left|\frac{\overline{\partial\rho}}{\partial t}\right| = s\left[w\frac{\partial\rho}{\partial z}\right], \tag{8}$$

where $s[A] \equiv \sqrt{[\overline{A}^2 - \overline{A}^2]}$ and the overbar denotes a temporal and spatial mean. If the numerical scheme were to preserve exactly the reversibility of the flow, this would not result in significant mixing, but in a typical depth-coordinate model there will be generally a net diffusive exchange of watermass properties across a density surface as a result of this transient flow. An associated advective diapycnal velocity g_{adv} may then be defined by dividing by the mean stratification:

$$g_{adv} \equiv s\left[w\frac{\partial\rho}{\partial z}\right] / \frac{\overline{\partial\rho}}{\partial z} \tag{9}$$

g_{adv} is essentially the standard deviation of the vertical velocity, weighted by the stratification, and represents the potential of the transient vertical velocity primarily to advect density, and ultimately to perform numerical mixing. Although we do not have any *a priori* quantification of what fraction of the numerical advection is irreversible, it is instructive to compare g_{adv} with the total diapycnal velocity g_{dia} from mixing, diagnosed earlier from the isopycnal drift and the divergence of the overturning streamfunction in density space (Eq. (6), and shown in Fig. 3). The ratio of these quantities may be interpreted as the fraction of the transient advection that is irreversible.

In Fig. 10 show the mean and standard deviation of the vertical velocity, the advective diapycnal velocity g_{adv} as defined in Eq. (9) and the ratio of the latter to the diagnosed diapycnal velocity g_{dia} from Section 4, all in density classes from 5-day means and then averaged in time. The time-mean vertical velocity (Fig. 10(a)) over much of the ocean is downward and less than 2×10^{-7} m s^{-1}, with the exception of the Equator, the Southern Ocean and the subpolar North Atlantic, where there is a mean upwelling of 10–20 $\times 10^{-7}$ m s^{-1}. The standard deviation of w (Fig. 10(b)) again can be seen to be an order or two of magnitude larger than the mean (note the different ranges on the colour scales), and is up to 1000 $\times 10^{-7}$ m s^{-2} (10 m/day) in the tropics and

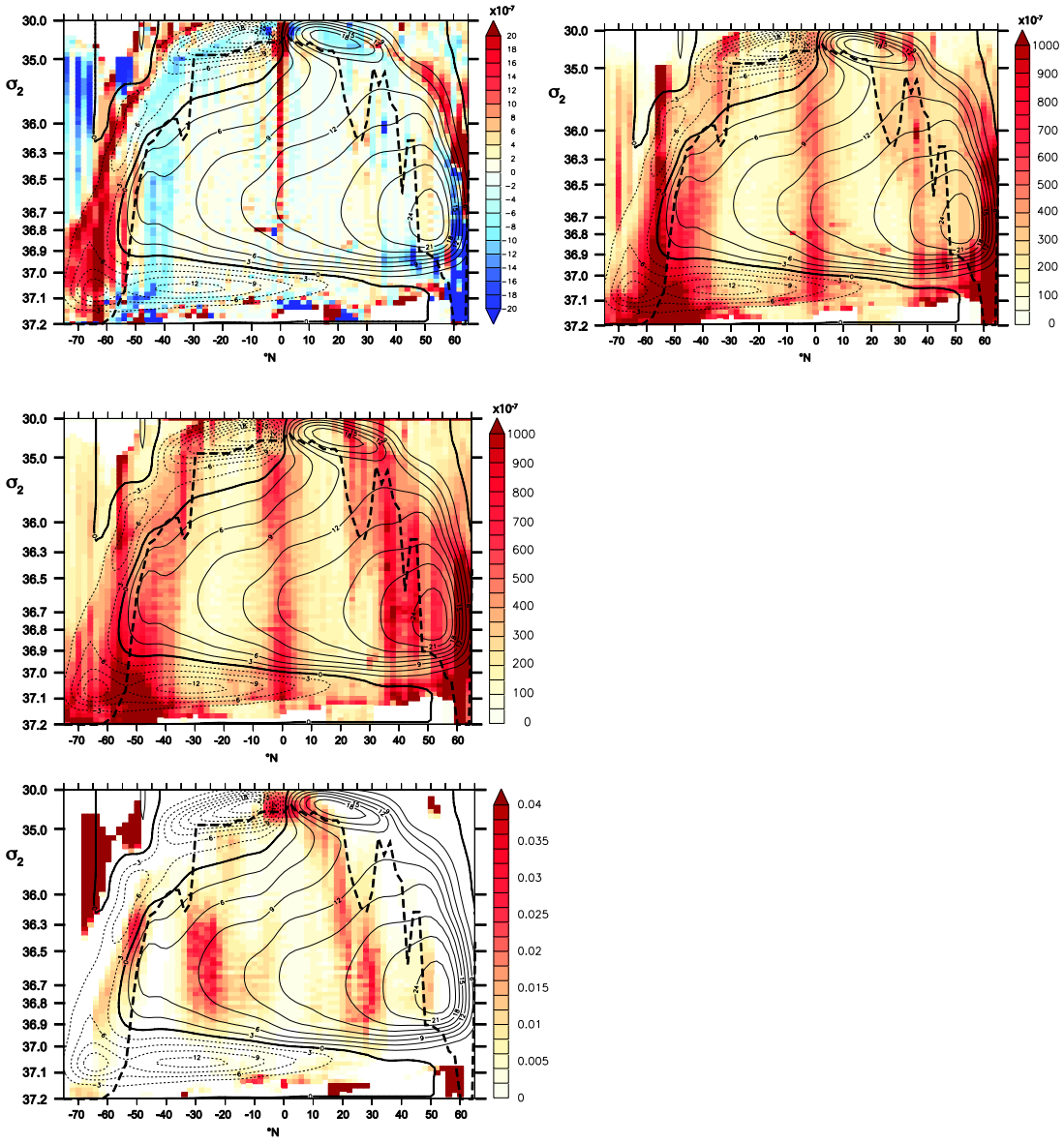

Fig. 10. (a) The mean vertical velocity ($\times 10^{-7}$ m s^{-1}) in density classes in the global domain; (b) its standard deviation; (c) the standard deviation of the effective advective diapycnal velocity; and (d) the ratio of the diagnosed diapycnal velocity to the latter.

subpolar regions, and with values generally higher below $\sigma_2 = 36.9$ (lower deep waters and bottom waters). The advective diapycnal velocity g_{adv} (Fig. 10(c)) has a similar magnitude and spatial distribution to the standard deviation, but is further enhanced in the regions where the w variance is large, especially in the North Atlantic between 35° and 50°N. Comparison between Figs. 5(b) and 10(c) shows that the spatial distribution of g_{adv} is strikingly similar to that of the diagnosed diapycnal velocity g_{dia}, particularly in the tropics and northern hemisphere, with large values close to the line of maximum surface density, as well as at all densities near the Equator and north of 30°N. To quantify this, Fig. 9(d) shows the ratio of g_{adv} *to* the diapycnal transformation rate g_{dia}: this is generally less than a percent, but has values of 2–3% in the ocean interior in the latitude ranges 35° − 20°S and 20–30°N. This suggests that the irreversible part of the numerical vertical advection in this model configuration typically constitutes a few percent of the total. The regions with the highest ratios are in the subtropics between 20° and 35°N and S, and correspond quite closely to the two regions in subtropical latitudes with the high ratios of numerical to explicit diffusivity (Fig. 8(a)), suggesting that these transient vertical velocities are at least partly responsible for the excessive mixing there.

5.3. Identification of high-frequency vertical motions

Blaker et al. (2012) analysed a comparable ¼° integration of NEMO, likewise forced by 6-hourly winds, and identified energetic near-inertial gravity waves (NIGWs) originating in the western boundary currents. These are initiated by intense wind events close to the western boundary and propagate towards the Equator. They have high vertical coherence between the thermocline and the ocean bottom and have periods close to the inertial period, wavelengths of 150–200 km, and are characterised with vertical velocities between ± 50 and 100 m/day. Their maximum amplitude in the Atlantic is between 25°N and 45°N, coinciding with the peaks of effective diffusivity described in Section 4. The 15–30 h period of the NIGWs in this latitude range means that they would not be appreciably detectable in the 5-day output of the integration discussed here, and this in turn implies that the vertical velocities shown in Figs. 9 and 10 significantly underestimate the transient vertical velocity field. To illustrate this, Fig. 11 shows the vertical velocities at 2000 m depth and on a section at 55°W, with scales chosen

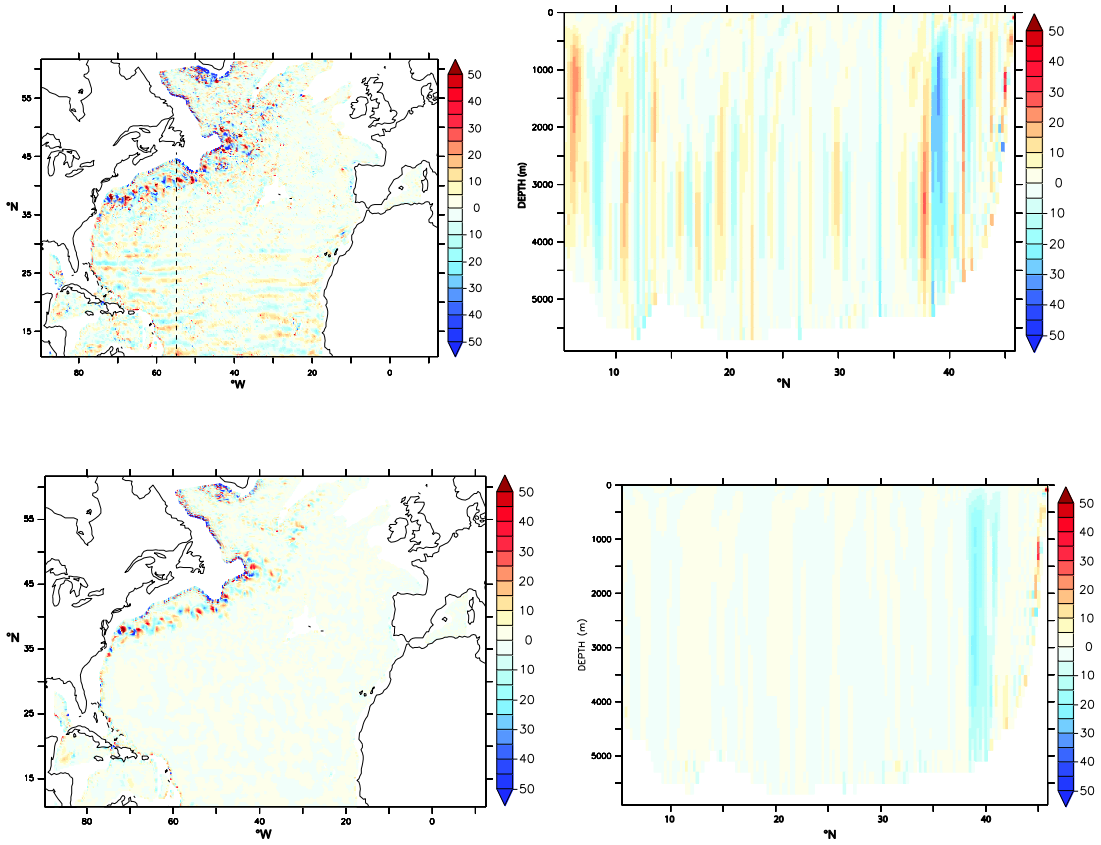

Fig. 11. (a) The instantaneous vertical velocity in metres per day at (a) 2000 m depth and (b) on a section at 55°W; the 5-day mean vertical velocity at (c) 2000 m depth; and (d) on a section at 55°W. The position of the section is shown by a dashed line in Fig. 10(a).

to render easy comparison with Fig. 5 of Blaker et al. Fig. 11(a) and (b) is an instantaneous field taken from a restart file from September of year 20 of the GO5.0 integration, while Fig. 11(c) and (d) is the mean vertical velocity over a five-day period including the instantaneous restart. In the instantaneous fields, zonal wavefronts can be seen south of 30°S with amplitude of up to 25 m/day, as well as eddy-like and noise-like features with substantially larger magnitudes close to the western boundary, north of 35°N. We remark that the corresponding figure in Blaker et al. shows vertical velocities of up to 100 m/day; the authors of that paper note the seasonality of the NIGWs, and the arbitrarily selected date of the output data shown in Fig. 10 may underrepresent the typical amplitude of these waves. By contrast, the 5-day mean only shows the downward flow of the deep western boundary current at 40°N and a few noise-like features near the shelf, with the NIGWs not visible at all on this scale. Comparison of the magnitudes of vertical motions in the two timescales confirms that the 5-day averaging causes an underestimate of the short-timescale vertical velocity field by up to an order of magnitude.

Griffies et al. (2000) suggest a direct relationship between numerical mixing and the vertical Courant number $w\Delta t/\Delta z$; as we have argued above, the stratification will also affect the potential of transient motions to cause numerical mixing, but intuitively we might expect the proportion of irreversible advection to be related to the fraction of a grid cell across which advection carries a water parcel in a single time step. The vertical grid spacing around 2000 m depth is about 150 m; the resolved vertical velocity of 25 m/day noted above corresponds to a displacement of 40 cm in a 1350-second model timestep, and a vertical Courant number of $2.5\text{x}10^{-3}$. In Section 5.2 we estimated the proportion of irreversible advection in those regions where the diagnosed diapycnal diffusivity is large compared with the explicit diffusivity to be of order 10^{-2}; that the vertical Courant number in these regions is of the same order of magnitude is then unsurprising.

6. Summary and discussion

We have applied the analysis of Lee et al. (2002), itself based on the isopycnal watermass transformation framework of Walin (1982) to diagnose the effective diapycnal diffusivity κ_{eff} in GO5.0, a 0.25° global ocean-only configuration of the NEMO model. The diffusivity, expressed as a function of potential density and latitude, is compared with that prognosed by the model's vertical mixing scheme, and it is found that in intermediate and deep water density classes, and on the Equator and in subtropical latitude bands, the values are up to an order of magnitude larger than the explicit diffusivity. Since the latter is set by the mixing scheme of the model to give a diffusivity with a magnitude and geographical distribution consistent with observational estimates, our results imply that the diapycnal mixing of the model is excessive, and that it is dominated by numerical mixing. As a further check, the diapycnal velocity, again diagnosed from the overturning circulation in density space, is compared with that derived from the explicit diffusivity and with observational estimates of mixing, and the former is also found to be up to ten times the explicit diapycnal velocity.

The standard deviation of the vertical velocity is found to have much larger magnitude than the mean vertical velocity, with values of up to 10 m/day in the ocean interior in the subpolar and equatorial regions. We have defined an effective advective diapycnal velocity as the vertical density advection divided by the density gradient, which, although quantitatively similar to the vertical velocity, explicitly represents the potential of transient motions to perform mixing. This again is found to have large values in the same latitude and density ranges as the largest diagnosed diapycnal velocities, namely the subpolar and equatorial regions and the deep and intermediate waters. We interpret this as evidence that these wavelike or eddy-like features are responsible for numerical mixing. The ratio of the effective advective diapycnal velocity to the diapycnal velocity derived directly from the

watermass transformation rate is found to be generally less than 1%, but has values of a few percent in the northern and southern subtropics in density classes containing upper deep waters and lower intermediate waters; in these watermasses the diagnosed diapycnal diffusivity was found to exceed the explicit diffusivity by a factor of 5–10, and we interpret this result as indicating that in these regions there is significant irreversibility in the vertical advection. We may assume that the numerical diffusion described here in the GO5.0 configuration of the NEMO model is by no means untypical of z-coordinate models with comparable resolution.

The method used in this paper is successful where the watermass transformation in density space is from denser to less dense water classes, consistent with a diffusive flow regime. On the large scale, in other words that of the global deep water and bottom water overturning cells, this is true over most of the model domain: in particular, we find that the North Atlantic Deep Water (NADW) has a nearly monotonic transformation rate as it travels southward and mixes with overlying intermediate waters, starting with a density of around $\sigma_2 = 37.05\,\mathrm{kg\ m^{-3}}$ at 35°N and having around $36.95\,\mathrm{kg\ m^{-3}}$ at 45°S. We have shown that adding a compensating term for the model drift, in the form of a rate of change of isopycnal volumes as in Lee et al. (2002), indeed removes some of these instances at higher densities, but there are still some remaining regions of apparently "anti-diffusive" flow, and in these cases the method described here fails to return a positive-definite value for the diffusivity. The regions of negative diffusivity in the Southern Ocean and North Atlantic correspond to the regions characterised by high rates of transformation due to cabbeling and thermobaricity by Klocker and McDougall (2010) and we tentatively ascribe these negative values to densification by these processes. The negative κ_{eff} in the tropical south Atlantic, however, is more likely to be non-physical, and is probably a result either of omitting short-timescale eddy motions in the volume transports or of truncation errors in space.

We have shown that there are large transient vertical velocities in the model with high coherence over the ocean depth, which take the form of noise-like features with length scales close to the model grid at subpolar latitudes, eddy-like structures near strong mean flows such as separated western boundary currents and the ACC, and near-inertial gravity waves with periods shorter than the five-day averaging period of the model output. These have amplitudes of 25–50 m/day, and Courant numbers of one or two percent. We have defined an advective diapycnal velocity g_{adv} as the standard deviation of the vertical advection of density, divided by the vertical density gradient, and interpret this as the potential of transient flows to advect density gradients. A fraction of this advection will be irreversible, as a result of truncation in the numerical advection scheme. This has a large-scale spatial structure similar to that of the diagnosed diapycnal velocity and in those regions where there is substantial numerical mixing the latter is found to have values of a few percent of the advective diapycnal velocity, confirming that the irreversible fraction of the numerical advection is of this order.

The high levels of small length-scale transient features in the vertical velocity in GO5.0 may or may not be realistic. Certainly the presence of poorly resolved quasi-mesoscale features in subpolar latitudes and in shallow coastal waters is undesirable, and this variability may be reduced by increasing the bilaplacian viscosity or by changing to an alternative parameterisation that is even more focused on the finest length scales, such as that of Smagorinsky (1963). The better resolved mid-latitude mesoscale eddies, the near-inertial gravity waves and the equatorial instability waves are likely to reflect corresponding features in the ocean, but their associated vertical displacements will nevertheless entail strong advection across coordinate surfaces with the potential to perform numerical mixing. LeClair and Madec (2011) formulated a scheme ("z-tilde") that permits short-timescale (periods less than a few days) deformations in the vertical coordinate, in analogy with isopycnal heave in the real ocean, allowing fast waves to propagate without significant vertical advection, and showed that this scheme led to a reduction in numerical mixing of up to a factor of five. This option was not available in Version 3.4 of NEMO as used in GO5.0, but is present in the latest release of Version 3.6.

The use of a higher-order vertical advection scheme improves the effective vertical resolution of the model (James, 2000) and hence is likely to reduce the magnitude of numerical mixing. Such schemes have been implemented in HYCOM, which allows piecewise constant, piecewise linear, and piecewise parabolic methods (PCM, PLM and PPM, respectively) to interpolate between vertical levels within a given water column, with increasing order of interpolation leading to less diffusion during the regridding of the hybrid vertical coordinate in that model (Bleck, unpublished manuscript). A piecewise parabolic method is currently available in NEMO, and we expect that this may well ameliorate the numerical mixing described here.

In summary, we have identified large amounts of numerical mixing in an eddy-permitting global ocean configuration based on a widely-used ocean model, NEMO. We stress that this does not implicate NEMO specifically, since the handling of the vertical coordinate in other depth-coordinate models is likely to be similar. The fact that closely-related configurations are now being used in climate models and earth system models aimed at CMIP6 implies that the drifts in the ocean temperature and salinity fields in such models, on time scales from decades to centuries, will bear a significant imprint of the numerical mixing. This weakness of this model class is particularly highlighted by the development of the hybrid isopycnal-coordinate model HYCOM, which has much-reduced numerical mixing, and more recently of generalised-coordinate (arbitrary Lagrangian–Eulerian) models such as the GFDL MOM6, in which the vertical coordinate may be optimised for different ocean regimes and which may be made quasi-isopycnal in the ocean interior. Methods to ameliorate the spurious mixing in a depth-coordinate model, whether by making the vertical advection scheme less diffusive or by permitting quasi-Lagrangian elastic displacements of coordinate surfaces on short timescales, are now available, and can only lead to improvements in the performance of the ocean model in both forced and coupled modes.

Acknowledgements

This work was funded by Natural Environment Research Council (UK) National Capability Funding. The author would like to thank George Nurser for his vital input and encouragement, and also Remi Tailleux, Gurvan Madec and Bablu Sinha for their many helpful suggestions. The manuscript was also substantially improved thanks to the suggestions of the two anonymous reviewers. The model was integrated on the MONSooN system, a collaborative facility supplied under the Joint Weather and Climate Research Programme, which is a strategic partnership between the Met Office and the Natural Environment Research Council, and was carried out under the Joint Ocean Modelling Programme (JOMP).

References

Barnier, B., Madec, G., Penduff, T., Molines, J.-M., Treguier, A.-M., Le Sommer, J., Beckmann, A., Biastoch, A., Böning, C., Dengg, J., Derval, C., Durand, E., Gulev, S., Remy, E., Talandier, C., Theetten, S., Maltrud, M., McClean, J., De Cuevas, B., 2006. Impact of partial steps and momentum advection schemes in a global ocean circulation model at eddy permitting resolution. Ocean Dyn. 56, 543–567. http://dx.doi.org/10.1007/s10236-006-0082-1.

Blaker, A.T., Hirschi, J.J-M., Sinha, B., de Cuevas, B., Alderson, S., Coward, A., Madec, G., 2012. Large near-inertial oscillations of the Atlantic meridional overturning circulation. Ocean Model. 42, 50–56. http://dx.doi.org/10.1016/j.ocemod.2011.11.008.

Bleck, R., Smith, L.T., 1990. A wind-driven isopycnic coordinate model of the North Atlantic and Equatorial Atlantic Ocean. I. Model development and supporting experiments. J. Geophys. Res. 95, 3273–3286.

Bleck, R., 2002. An oceanic general circulation model framed in hybrid isopycnic-cartesian coordinates. Ocean Model. 37, 55–88.

Blockley, R.E.W., Martin, M.J., McLaren, A.J., Ryan, A.G., Waters, J., Lea, D.J., Mirouze, I., Peterson, K.A., Sellar, A., Storkey, D., 2014. Recent development of the Met Office operational ocean forecasting system: an overview and assessment of the new Global FOAM forecasts. Geosci. Model Dev. 7, 2613–2638. http://dx.doi.org/10.5194/gmd-7-2613-2014. http://www.geosci-model-dev.net/7/2613/2014/.

Burchard, H., Rennau, H., 2008. Comparative quantification of physically and numerically induced mixing in ocean models. Ocean Model. 20, 293–311.
Chen, C.-T., Millero, F.J., 1987. The equation of state for seawater determined from sound speeds. J. Mar. Res. 36 (4), 657–691.
Dunne, J.P., John, J., Adcroft, A., Griffies, S.M., Hallberg, R.W., Shevliakova, E., Stouffer, R.J., Cooke, W.F., Dunne, K.A., Harrison, M.J., Krasting, J.P., Malyshev, S., Milly, P.C.D., Phillipps, P., Sentman, L.T., Samuels, B.L., Spelman, M.J., Winton, M., Wittenberg, A.T., Zadeh, N., 2012. GFDL's ESM2 global coupled climate-carbon Earth System Models. Part I: Physical formulation and baseline simulation characteristics. J. Clim. 25 (19), 6646–6665. http://dx.doi.org/10.1175/JCLI-D-11-00560.1.
Gaspar, P., Grégoris, Y., Lefevre, J.-M., 1990. A simple eddy kinetic energy model for simulations of the oceanic vertical mixing: tests at Station Papa and long-term upper ocean study site. J. Geophys. Res. 95, 16179–16193. http://dx.doi.org/10.1029/JC095iC09p16179.
Gent, P.R., McWilliams, J.C., 1990. Isopycnal mixing in ocean circulation models. J. Phys. Oceanogr. 20, 150–155.
Getzlaff, J, Nurser ad, G., Oschlies, A, 2012. Diagnostics of diapycnal diffusion in z-level ocean models. Part II: 3-dimensional OGCM. Ocean Model. 45–46 (2012), 27–36.
Gregg, M.C., Sanford, T.B., Winkel, D.P., 2003. Reduced mixing from the breaking of internal waves in equatorial waters. Nature 422, 513–515.
Griffies, S.M., Pacanowski, R.C., Hallberg, R.W., 2000. Spurious diapycnal mixing associated with advection in a z-coordinate ocean model. Mon. Weather Rev. 128 (3), 538–564.
Griffies, S.M., Harrison, M.J., Pacanowski, R.C., Rosati, A., 2008. A Technical Guide to MOM4: GFDL Ocean Group Technical Report No. 5. Version prepared on 4 February, 2008. Available online at. http://www.gfdl.noaa.gov.
Grist, J.P., Marsh, R., Josey, S.A., 2009. On the relationship between the North Atlantic meridional overturning circulation and the surface-forced overturning streamfunction. J. Clim. 22, 4989–5002.
Hallberg, R., Adcroft, A., 2009. Reconciling estimates of the free surface height in Lagrangian vertical coordinate ocean models with mode-split time stepping. Ocean Model. 29, 15–26. http://dx.doi.org/10.1016/j.ocemod.2009.02.008.
Hofmann, M., Morales Maqueda, M.A., 2006. Performance of a second-order moments advection scheme in an ocean general circulation model. J. Geophys. Res.-Oceans 111 (C5).
Hunke, E.C., Lipscomb, W.H., 2010. CICE: The Los Alamos Sea Ice Model, Documentation and Software User's Manual, Version 4.1. Los Alamos National Laboratory, Los Alamos, New Mexico Technical Report LA-CC- 06-012. http://oceans11.lanl.gov/trac/CICE.
Ilıcak, M., Adcroft, A.J., Griffies, S.M., Hallberg, R.W., 2012. Spurious dianeutral mixing and the role of momentum closure. Ocean Model. 45–46, 37–58.
IPCC, 2013. Climate change 2013: the physical science Basis. In: Stocker, T.F., Qin, D., Plattner, G.-K., Tignor, M., Allen, S.K., Boschung, J., Nauels, A., Xia, Y., Bex, V., Midgley, P.M. (Eds.), Contribution of Working Group I to the Fifth Assessment Report of the Intergovernmental Panel On Climate Change. Cambridge University Press, Cambridge, United Kingdom and New York, NY, USA, pp. 1535.
Jackett, D.R., McDougall, T.J., 1995. Minimal adjustment of hydrographic profiles to achieve static stability. J. Atmos. Ocean. Technol. 12 (4), 381–389.
James, I.D., 2000. A high-performance explicit vertical advection scheme for ocean models: how PPM can beat the CFL condition. Appl. Math. Model. 24, 1–9.
Klocker, A., McDougall, T.J., 2010. Influence of the nonlinear equation of state on global estimates of dianeutral advection and diffusion. J. Phys. Oceanogr. 40, 1690–1709.
Kraus, E.B., Turner, J.S., 1967. A one-dimension model of the seasonal thermocline. II: The general theory and its consequences. Tellus 19, 98–106.
Kunze, E., Firing, E., Hummon, J.M., Chereskin, T.K., Thurnherr, A.M., 2006. Global abyssal mixing inferred from lowered ADCP shear and CTD strain profiles. J. Phys. Oceanogr. 36, 1553–1576. http://dx.doi.org/10.1175/JPO2926.1.
Large, W.G., McWilliams, J.C., Doney, S.C., 1994. Oceanic vertical mixing: a review and a model with a nonlocal boundary layer parameterization. Rev. Geophys. 32, 363–403.
Large, W.G., Yeager, S.G., 2009. The global climatology of an interannually varying air–sea flux data set. Clim. Dyn. 33, 341–364. http://dx.doi.org/10.1007/s00382-008-0441-3.
LeClair, M., Madec, G., 2011. z^{-}-Coordinate, an arbitrary Lagrangian–Eulerian coordinate separating high and low frequency motions. Ocean Model. 37, 139–152.
Lee, M.-M., Coward, A.C., Nurser, A.G., 2002. Spurious diapycnal mixing of deep waters in an eddy-permitting global ocean model. J. Phys. Oceanogr. 32, 1522–1535.
Legeckis, R., 1977. Long waves in the eastern equatorial Pacific Ocean: a view from geostationary satellite. Science 197, 1179–1181.
Luyten, J.R., Pedlosky, J., Stommel, H., 1983. The ventilated thermocline. J. Phys. Oceanogr. 13, 292–309.
Madec, G., 2016. NEMO – The OPA9 Ocean Engine: Note du Pole de Modelisation. Institut Pierre-Simon Laplace No. 27, Available at. https://www.nemo-ocean.eu/wp-content/uploads/NEMO_book.pdf ISSN 1288-1619, last access: 4 July 2017.
Marsh, R., 2000. Recent variability of the North Atlantic thermohaline circulation inferred from surface heat and freshwater fluxes. J. Clim. 13, 3239–3260.
Marsh, R., Nurser, A.J.G., Megann, A.P., New, A.L., 2000. Water mass transformation in the Southern Ocean of a global isopycnal coordinate GCM. J. Phys. Oceanogr. 30, 1013–1045.
Megann, A.P., New, A.L., Blaker, A.T., Sinha, B., 2010. The sensitivity of a coupled climate model to its ocean component. J. Clim. 23, 5126–5150.
Megann, A., Storkey, D., Aksenov, Y., Alderson, S., Calvert, D., Graham, T., Hyder, P., Siddorn, J., Sinha, B., 2014. GO5.0: The joint NERC-Met Office NEMO global ocean model for use in coupled and forced applications. Geosci. Model Dev. 7, 1–24.
Munk, W., Wunsch, C., 1998. Abyssal recipes II: energetics of tidal and wind mixing. Deep-Sea Res I 45, 1977–2010.
Nurser, A.J.G., Lee, M-M., 2004. Isopycnal averaging at constant height. Part I: the formulation and a case study. J. Phys. Oceanogr. 34, 2721–2739.
Smagorinsky, J., 1963. General circulation experiments with the primitive equations: part I, the basic experiment. Mon. Weather Rev. 91, 99–164.
Walin, G., 1982. On the relation between sea-surface heat flow and thermal circulation in the ocean. Tellus 34, 187–195.
Waterhouse, A.F., MacKinnon, J.A., Nash, J.D., Alford, M.H., Kunze, E., Simmons, H.L., Polzin, K.L., St Laurent, L.C., Sun, O.M., Pinkel, R., Talley, L.D., Whalen, C.B., Huussen, T.N., Carter, G.S., Fer, I., Waterman, S., Naveira Garabato, A.C., Sanford, T.B., Lee, C.M., 2014. Global patterns of diapycnal mixing from measurements of the turbulent dissipation rate. J. Phys. Oceanogr. 44 (7), 1854–1872.
Williams, K.D., Harris, C.M., Bodas-Salcedo, A., Camp, J., Comer, R.E., Copsey, D., Fereday, D., Graham, T., Hill, R., Hinton, T., Hyder, P., Ineson, S., Masato, G., Milton, S.F., Roberts, M.J., Rowell, D.P., Sanchez, C., Shelly, A., Sinha, B., Walters, D.N., West, A., Woollings, T., Xavier, P.K., 2015. The Met Office Global Coupled model 2.0 (GC2) configuration. Geosci. Model Dev. 88, 1509–1524. http://dx.doi.org/10.5194/gmd-88-1509-201. www.geosci-model-dev.net/88/1509/2015/.
Williams, KD, Copsey, D., Blockley, E., Bodas-Salcedo, A., Calvert, D., Comer, R., Davis, P., Graham, T., Hewitt, HT., Hill, R., Hyder, P., Ineson, S., Johns, TC., Keen, A., Lee, RW., Megann, A., Milton, S.F., Rae, J., Roberts, MJ., Scaife, A.A., Schiemann, RK., Storkey, D., Thorpe, L., Watterson, IG., Walters, DN., West, A., Wood, R., Woollings, T., Xavier, PK., 2017. The Met Office Global Coupled model 3.0 and 3.1 (GC3 & GC3.1) configurations. J. Adv. Model. Earth Syst under review.
Zalesak, S.T., 1979. Fully multidimensional flux corrected transport algorithms for fluids. J. Comput. Phys. 31, 335–362.